Fully Optical in Operando Investigation of Ambient Condition Electrical Switching in MoS₂ Nanodevices

Joanna Symonowicz, Dmitry Polyushkin, Thomas Mueller, and Giuliana Di Martino*

MoS₂ nanoswitches have shown superb ultralow switching energies without excessive leakage currents. However, the debate about the origin and volatility of electrical switching is unresolved due to the lack of adequate nanoimaging of devices in operando. Here, three optical techniques are combined to perform the first noninvasive in situ characterization of nanosized MoS₂ devices. This study reveals volatile threshold resistive switching due to the intercalation of metallic atoms from electrodes directly between Mo and S atoms, without the assistance of sulfur vacancies. A "semi-memristive" effect driven by an organic adlayer adjacent to MoS₂ is observed, which suggests that nonvolatility can be achieved by careful interface engineering. These findings provide a crucial understanding of nanoprocess in vertically biased MoS₂ nanosheets, which opens new routes to conscious engineering and optimization of 2D electronics.

1. Introduction

Electrical switches based on MoS₂ nanosheets have attracted a lot of attention[1–20] due to their ultralow switching energies[14,20] without excessive leakage currents for few-nanometers thick devices.[13,16] Moreover, some of them exhibit nonvolatile (memristic) switching[12,14,17] which facilitates neuromorphic computing capable of reducing energy consumption in IT by up to 80%.[21,22] Nevertheless, most groups observe only a volatile effect[23–26] and nonvolatility is achieved by oxidation[6,12] and sulfurization of MoS₂ bulk[5] or by stacking MoS₂ monolayers.[17]

To achieve commercial importance, vertical nanoscale devices (with areas < 10^4 nm²) are desirable, as they provide the lowest switching voltages and highest integration densities.[27] On the contrary, most of the switching behaviors are studied in microsized devices[1–17] although stochastic switching processes are different for microscale and nanoscale electrodes.[27] To our knowledge, only two works investigate MoS₂ biased vertically with nanosized electrodes.[18,20] Both report volatile conductive filaments formed by metallic atoms diffusing from electrodes into sulfur vacancies (V_S).[18,20] However, those measurements are performed in vacuum conditions, again leading to different switching dynamics and device performances of the ones observed in the air.[13,18,20,27] Therefore, due to the lack of adequate imaging technologies capable of peering into commercially relevant devices, i.e., at the nanoscale and in ambient conditions, the origin and the volatility of electrical switching in MoS₂ remains unclear.[16,27]

We have recently developed the first non-invasive technique able to track material's morphology in situ, at the nanoscale, and in ambient conditions, via plasmon-enhanced dark field (DF) nanospectroscopy.[28–30] Here, we expand it with additional capabilities offered by nano-Raman and nano-photoluminescence to study the switching mechanism in MoS₂. The method's principle is presented in **Figure 1**a. An 80 nm gold nanoparticle (AuNP) placed in the vicinity of a gold substrate is illuminated with white light ($\lambda \approx 400$–900 nm) to produce plasmonic resonances within the AuNP (single mode) and in a spacer between AuNP and the substrate (gap mode).[31,32] The resonances are detected using DF scattering microscope configuration and the gap mode's wavelength and intensity depend on the spacer's refractive index, thickness, and geometry.[31,32] Using a AuNP as a nanosized (≈700 nm²) top contact of an electrical switch[29,33] results in a strong field enhancement localized within the nanoscale switching channel. This greatly enhances both Raman and photovluminescence (PL) signals,[34] conveniently highlighting the otherwise undetectable nanoscale switching dynamics.

Many switching mechanisms are proposed in the literature for MoS₂, as summarized in **Table 1**. Among these are migrations of sulfur vacancies (V_S),[3,9,10] movements of oxygen in oxidized MoS₂,[6,12] charge trapping and detrapping,[2] phase change from semiconducting (2H) to metallic (1T'),[4,7] and metal ions intercalating from electrodes.[5,13,17,18,20] We note that all the above mechanisms would trigger changes in optical signals (Raman, PL) which are detectable with our experimental capabilities. In particular, the density of V_S, which are observed in all MoS₂ nanosheets studied by transmission electron microscopy (TEM),[36–38] is correlated to the PL peak at ≈750 nm,[39,40] the intensity ratio of MoS₂'s A/B excitons[39,41]

J. Symonowicz, G. Di Martino
Department of Materials Science and Metallurgy
University of Cambridge
27 Charles Babbage Rd, Cambridge CB3 0FS, UK
E-mail: gd392@cam.ac.uk
D. Polyushkin, T. Mueller
Vienna University of Technology
Institute of Photonics
Gusshausstrasse 27–29 / 387, Vienna 1040, Austria

The ORCID identification number(s) for the author(s) of this article can be found under https://doi.org/10.1002/adma.202209968.
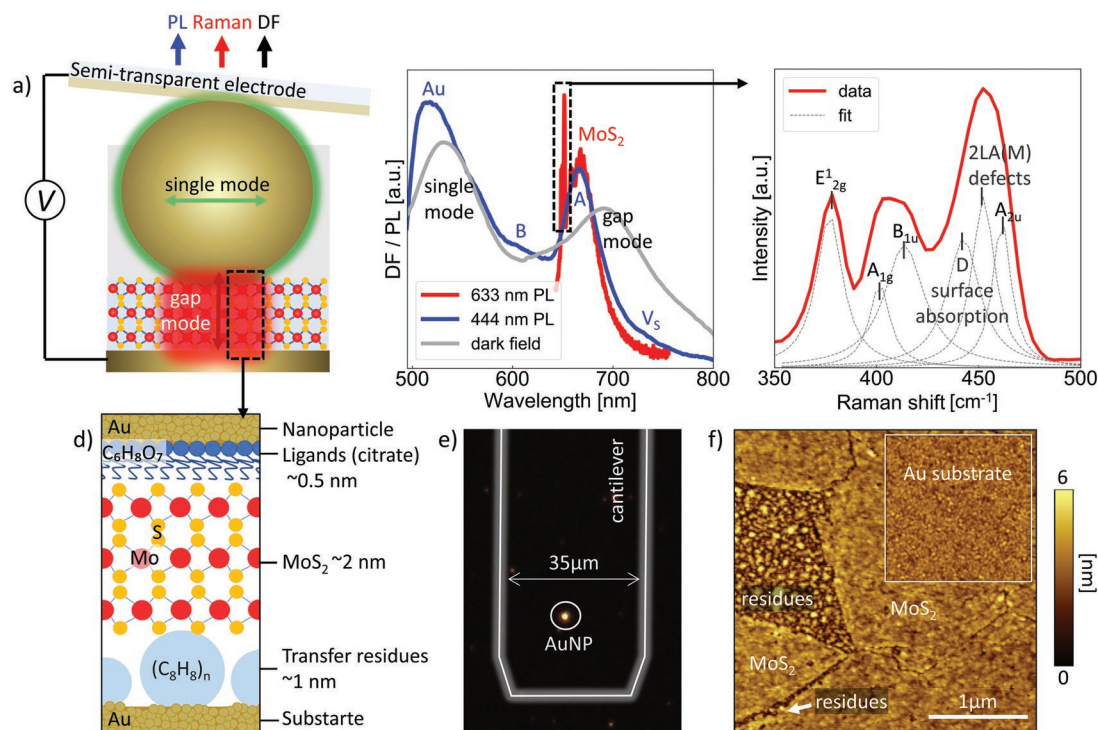
Figure 1. a) Device layout. b) Optical characterization of MoS$_2$ switch by white light (DF), 633 nm laser (PL, Raman – marked by a dashed rectangle) and 444 nm laser (PL) illumination. The plasmonic gap mode enhances MoS$_2$'s PL, while the single mode boosts Au luminescence. c) Zoom on the resonant Raman part of the 633 nm excitation.[35] d) Scheme of a switching channel: MoS$_2$ is sandwiched between transfer residues and ligands. e) Dark field microscopy picture of the device contacted by a cantilever. f) AFM map of MoS$_2$ before the deposition of nanoparticle top electrodes. Rough surface under MoS$_2$ suggests polymer residues and not substrate damage, as verified by examining Au substrate in the area without MoS$_2$ (insert).

and the separation between A$_{1g}$ and E$^1_{2g}$ Raman modes.[39,42] V$_S$ and V$_O$ p-dope MoS$_2$ quenching PL[40,43] and hence switching processes associated with n-doping (charge trapping[2,6,11] and V$_O$ migration[6,12]) would mitigate the drop in PL.[40,43,44]

Moreover, n-doping modifies A$_{1g}$ Raman mode.[45] Electrical switching triggered by phase transitions or adsorption of water/air[6] would result in new Raman peaks.[4,7,35,46] Lastly, intercalation of Au into MoS$_2$ would quench optical signals.[20,47]

Table 1. Review of mechanisms explaining resistivity changes in MoS$_2$ nanoswitches, with expected changes in Raman and PL spectra of MoS$_2$.

Proposed mechanism	Diagram	Expected changes in Raman	Expected changes in PL
Metal intercalation into V$_S$.[5,13,17,18,20]		Signal quenched by contact with Au.[48] Modification of A$_{1g}$ and 2LA(M) modes associated with V$_S$.[42,49,50]	Signal quenched by contact with Au.[20,47] Modification of V$_S$ peak at ≈750 nm.[39,40]
V$_S$ migration near grain boundaries.[3,9,10]		Surge in V$_S$ increases separation between A$_{1g}$ and E$^1_{2g}$ modes.[42]	Risen V$_S$ gives new peak at ≈750 nm,[39,40] quenches PL,[39] reduces A/B exciton ratio.[39,41]
Phase change from 2H to 1T′.[4,7]		Raman modes for 1T′: 200, 225, 355 cm^{-1}; modes for 2H: 384, 408 cm^{-1}.[4,46]	1T′ metallic phase shows PL.[46]
Migration of oxygen defects in oxidized MoS$_2$.[6,12,51]		Absorption of O$_2$ produces mode at ≈440 cm^{-1}[35] and blue-shifts A$_{1g}$ mode.[43]	Absorption of O$_2$ boosts PL's intensity.[43,44]
Charge trapping and detrapping.[2,6,11]		n-doping softens and broadens A$_{1g}$ mode.[42]	n-doping enhances PL because MoS$_2$ is naturally p-doped by V$_S$.[40,52]

Our aim is to investigate morphological changes occurring in electrically biased MoS_2 nanosheets by spectroscopical observation of defects dynamics. Here, for the first time, we not only access both PL and Raman in operando, but we additionally support those optical signatures with DF spectroscopy for a true real time investigation of MoS_2 switching mechanisms.

2. Results

2.1. Material Characterization

We fabricate cells by transferring MoS_2 onto Au substrate and drop-casting AuNP as a top electrode (see Figure 1a). The AuNP is electrically biased via a conductive but optically semi-transparent cantilever, as presented in Figure 1e. A scheme of electrical contacting setup is shown in Figure S1 in the Supporting Information.

Optical characterization of the MoS_2 switch (Figure 1b) is obtained both by broad incoherent white light illumination (400–900 nm) to investigate plasmonic resonances (DF), and laser irradiation to enable PL with two different excitation wavelengths (444 and 633 nm) and Raman with 633 nm excitation. DF scattering shows a gap mode at ≈700 nm and a single mode at ≈550 nm, enhancing PL emissions from MoS_2 (668, 615 nm[39,53]) and Au (525, 557 nm[54,55]), respectively. With 444 nm excitation laser, we observe a small peak at ≈740 nm in the PL signal which we attribute to V_S.[40]

MoS_2 excitons A and B (668 and 615 nm, respectively) are in resonance with the 633 nm laser wavelength which we use for our Raman characterization. As a result, we observe resonant Raman,[35] marked by a dashed rectangle in Figure 1b. It enhances the otherwise too dim Raman signal coming from just few layers of MoS_2 and enables observation of modes dynamics otherwise too weak to be tracked.[56] The collected resonant Raman is magnified in Figure 1c. It suggests the presence of V_S (mode 2LA(M) at 452 cm^{-1} activated by defects[49]) and residues bonded to MoS_2's surface (mode D at 440 cm^{-1}).[35] It can be further used to estimate MoS_2 thickness, as spacing between E^1_{2g} and A_{1g} modes is thickness dependent.[35] In the device presented in this work we find a spacing of 24 cm^{-1}, corresponding to three layers MoS_2, i.e., thickness of about 2 nm.[35,57] In total, we tested ≈40 cells with 1–3 layers of MoS_2 (verified by PL and Raman) and the change in optical signals with switching was analogous for all thicknesses.

Since moisture and fabrication residues influence electrical switches,[18,58] we make sure to consider all possible species present in our cell, as presented in Figure 1d. The residues are hardly ever mentioned in literature related to 2D materials because standard imaging techniques are either destructive to nanosized organics (electron microscopies) or residues signal is overshadowed by atmospheric contaminants (X-ray photoelectron and energy dispersive spectroscopies). Consequently, we use our novel optical technique, highlighting its clear advantage in transfer residues detection. It combines four independent methods, such as Raman, PL, DF, and atomic force microscopy (AFM). First, we consider residues associated with AuNP drop-casting. AuNPs are stabilized by citrate ligands ($C_6H_8O_7$)[59] and we confirm their presence by Raman and DF

measurements on a control sample consisting of AuNP drop casted directly on Au substrate (Figure S2, Supporting Information). The resulting DF mode's wavelength implies a gap of ≈0.5 nm, which matches literature values.[60] Second, we investigate possible organic transfer residues (polystyrene – $(C_8H_8)_n$) surrounding MoS_2.[61] We expect an adlayer between MoS_2 and Au because MoS_2's PL signal would be otherwise quenched by a direct contact with Au.[47] Indeed, AFM scans (Figure 1f; Figure S3, Supporting Information) reveal different surface roughness for MoS_2 (≈0.4 nm), Au substrate beneath MoS_2 (≈1.2 nm), and Au in region without MoS_2 (≈0.6 nm). Since the "bumps" on Au occur only in vicinity of MoS_2, we conclude that they are not due to damaged Au substrate but are polymer residues.[62] Smooth surface of MoS_2 indicates that polystyrene is surprisingly only under MoS_2 and not on top of it (see arrow in Figure 1f). Moreover, the AFM step of 2 nm (Figure S3a, Supporting Information) corresponds to three layers of MoS_2 (previously verified by Raman) which implies that no additional layer is present on top of MoS_2. Knowing that the combined thickness of MoS_2 + ligands is ≈2.5 nm (verified by Raman, DF, and AFM, see Figure 1c and Section SB in the Supporting Information), with FDTD framework we calculate that the observed resonance at ≈700 nm (Figure 1b) would require additional polymer thickness of ≈1 nm, which corresponds to the observed surface roughness (≈1.2 nm).

2.2. In Situ 444 nm Photoluminescence

We track the evolution of the PL signal (**Figure 2**a) while the device is biased with triangular field profiles between +/−5 V (Figure 2b). A link between PL intensity and applied voltage is present and further highlighted by averaging over many switching cycles (Figure 2c). The individual optical responses of Au, MoS_2 and V_S are extracted by Lorentzian fits (Figure 2c: blue, red, and grey for −5, 5, and 0 V, respectively). The most prominent change triggered by both positive and negative voltage is the rise in Au luminescence (≈540 nm), suggesting more Au atoms present in the gap between electrodes, i.e., Au intercalation into MoS_2. The 540 nm luminescence increase is greater for V < 0 when Au is pulled from a substrate rather than from AuNP, due to ligands surrounding the top AuNP limiting Au atoms drift. The PL peak at 740 nm, linked to V_S content,[39,40] is unaffected by voltage (insert in Figure 2c). Therefore, contrary to previous suggestions (Table 1),[13,18,20] V_S seem not to take part in the switching process. Although MoS_2's A and B excitons are visible in the collected data, they overlap with a strong Au luminescence background, which results in a Laurentian fitting characterized by statistical errors large enough to prevent making any conclusion on the MoS_2 PL behavior with voltage.

2.3. In Situ 633 nm Laser Excitations

To eliminate the effect of Au background, we additionally collect PL using a 633 nm excitation laser (**Figure 3**). The gain in using a 633 nm excitation laser is twofold as, on top of enabling in operando resonant Raman, it also allows focusing on the MoS_2
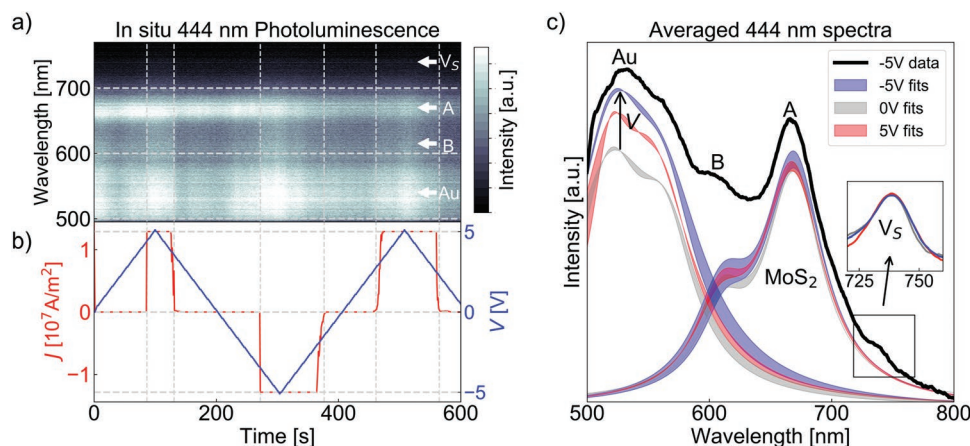
Figure 2. In situ PL characterization (444 nm excitation laser) of a vertically biased MoS$_2$ nanosheet: a) PL signal evolution in time, b) applied voltages with measured current densities (J), and c) PL spectra at 5, 0, and −5 V averaged over many switching cycles, with shadows indicating statistical errors in the fitting process.

PL without Au background, and specifically on the dynamics of exciton A with voltage. Our in situ PL/Raman studies highlight two important behaviors. First, the PL signal is quenched when the sample becomes conductive (Figure 3), implying Au is in direct contact with MoS$_2$.[20,47] Second, the advent of current does not shift the position of Raman peaks (Figure 3c – inset). We highlight that the passivation of V$_S$ would result in the PL increase with bias[40,52] and the shift of A$_{1g}$ Raman mode,[42] which is contrary to our findings. Those distinctive signatures confirm that V$_S$ do not contribute to the process. Furthermore, they eliminate all switching mechanisms proposed in the literature except for metallic ions intercalation but without mediation of V$_S$, contrary to the data presented in Table 1.

2.4. In Situ Darkfield Scattering

We complement our finding by investigating the evolution of the scattering signal with bias under white light illumination. This further expand the understanding of the switching mechanism, revealing the specific geometry of Au filaments

intercalating MoS$_2$. Once the device is ON (+/−5 V), the plasmonic gap mode at ≈690 nm is reduced in intensity and no spectral shift is observed (**Figure 4**a).

To understand the mechanism behind this observation we simulate the geometry of the system through a commercial software (*Lumerical*) based on a finite-difference time-domain (FDTD) method.[63] We consider and simulate two possible scenarios determined by applied voltage: the creation of one Au filament which increases its size from 0 to 10 nm in diameter (Figure 4b) and the growth of several (1–145), equally sized (0.1 nm) and equally spaced Au filaments (Figure 4c). They both capture the mode intensity reduction observed experimentally. In fact, this confirms the intuitive picture where the formation of a Au bridge allows electrons to pass through the gap leading to an effective shorting of the plasmonic field confinement, hence reduction of its intensity. The two scenarios differ in their mode shift. The increase in size of one single filament would lead to a pronounced peak shift (Figure 4b), which we do not observe experimentally (Figure 4a). On the contrary, the growth of several and equally sized and spaced Au filaments (Figure 4c), shows almost no shift (for >40 filaments a small field interaction
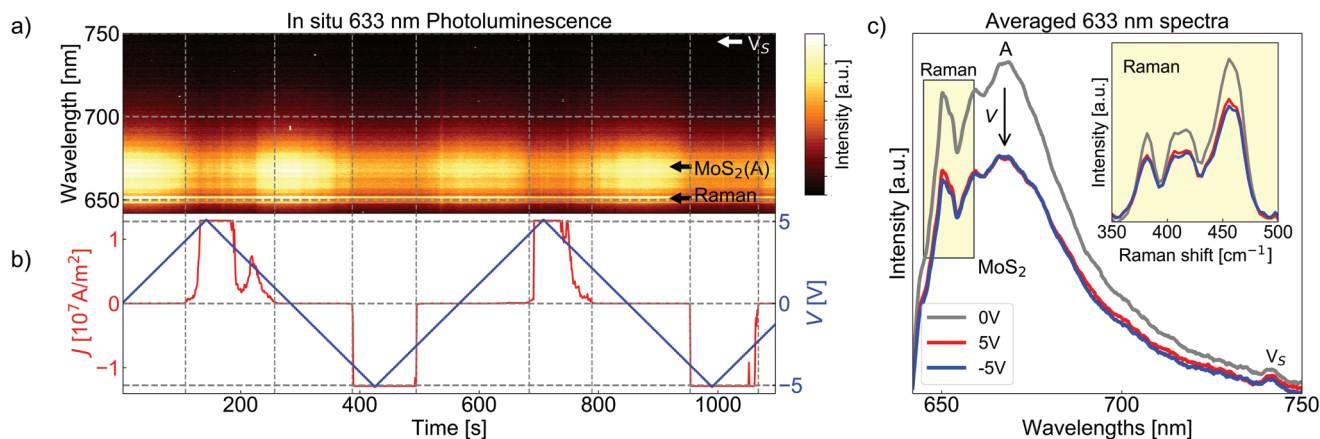
Figure 3. In situ PL/Raman (633 nm laser) characterization: a) optical signal time evolution, b) applied voltage profile with measured current density (J), and c) spectra for 5, 0, and −5 V averaged over many cycles. Inset: zoom on Raman spectra. Pulling of Au into MoS$_2$ by bias explains the observed quenching of PL and unshifted Raman signals.
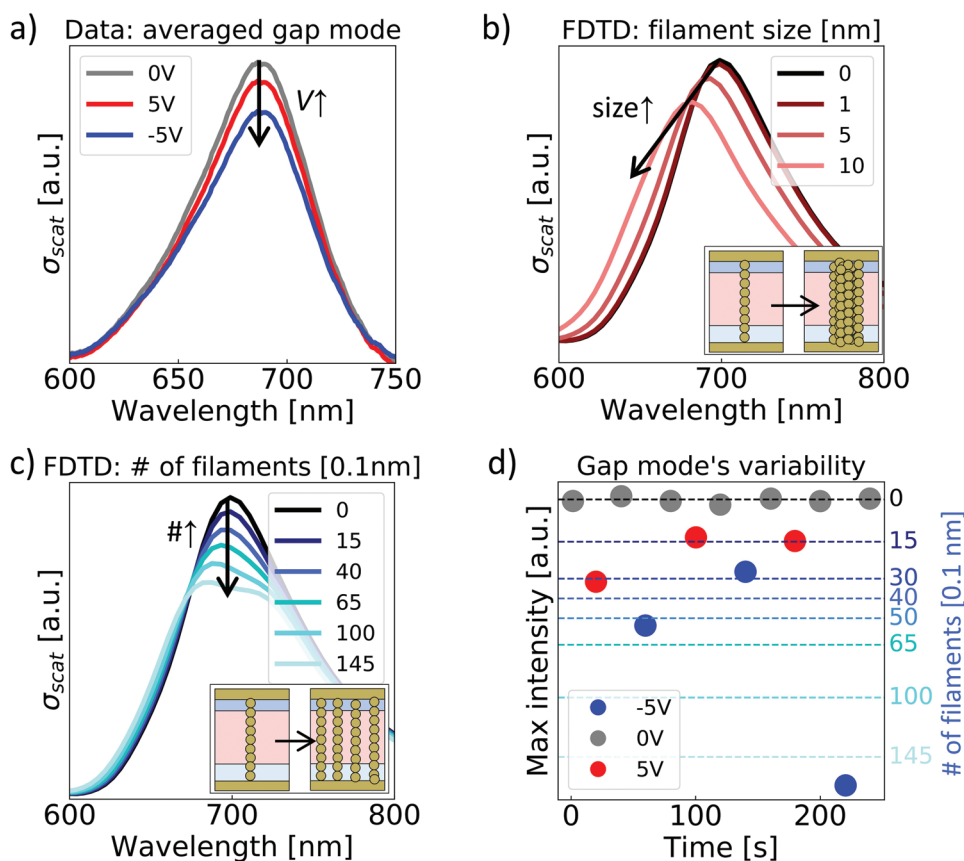
Figure 4. Dark field analysis of the MoS$_2$ switch. a) Gap resonance decreases with voltage (data averaged over many cycles). b,c) FDTD simulations when b) one Au filament increases its size (0–10 nm in diameter) and c) several (1–145), equally atomic-sized (0.1 nm) and equally spaced Au filaments grow. d) Difference in a gap mode intensity reduction for individual cycles when a different number of 0.1-nm-thick filaments percolate MoS$_2$ (left axis: experimental data, right axis: simulation).

between nearby filaments is starting to mimic the field effect of a unique large filament causing a very minimal spectral shift). Therefore, this would confirm the picture of many nanofilaments (1–2 Au atoms thick) penetrating spaces between atoms in MoS$_2$ rather than one filament (or few, see Figure S4 in the Supporting Information) growing along a grain boundary, enlarging with voltage. Direct intercalation of Au atoms into interatomic distances in MoS$_2$ is possible as the size of a Au atom is ≈1.4 Å[64] and the horizontal distance between atoms in the 2H phase of MoS2 is ≈3.2 Å.[65] Moreover, from our simulation we can estimate the number of filaments per each switching event, with a typical intensity reduction of ≈7% corresponding to ≈15 filaments in MoS$_2$. Therefore, we can investigate how the gap mode's intensity change over several cycle (Figure 4d), observing a considerable statistical variation. This suggests that a different number of filaments is pulled by the same voltages over different switching events. We note that the effect is mildly less stochastic when Au drift is halted by ligands (5 V).
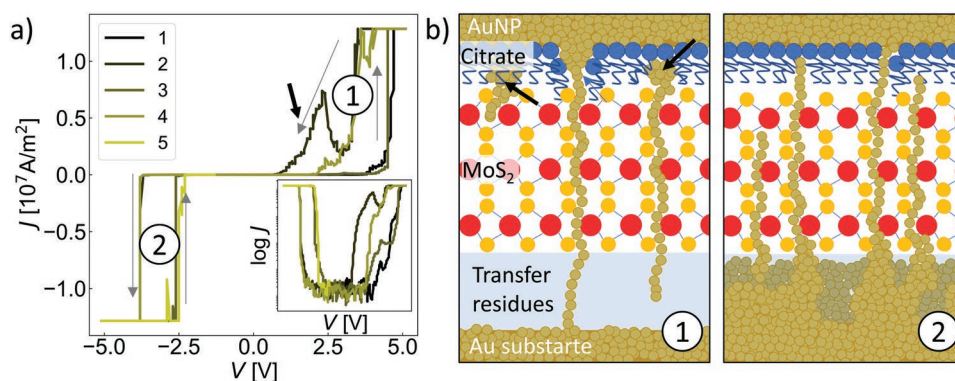
2.5. Electrical Characteristics

A typical current density–voltage ($J–V$) characteristic (**Figure 5**a) reveals threshold volatile resistive switching.[66] It is independent of a compliance level, and nonvolatility is not observed even when we use current densities above those suggested in literature for memristive switching.[18,67] Moreover, we do not observe electro-forming cycle. MoS$_2$ recovers an OFF state for $|V| < ≈2.5$ V. High switching voltages of 4–5 V are most likely due to adlayers. We verify it by repeating electrical characterization with microsized electrodes without ligands, for which we obtain same stochastic threshold behavior with lower voltages of 2–3 V (Figure S5, Supporting Information). We note that the switching timescale in our operando method is different from that of commercial devices, which may operate at high frequencies. However, our experiment, in which we stress MoS$_2$ with pulses, results in same stochastic volatile threshold switching as observed in slower $I–V$ scans (Figure S5, Supporting Information), matching $I–V$ scans for a statistic of devices (Figure S6, Supporting Information).

3. Discussion

The ON/OFF switching is more stochastic, less sharp, and requires ≈1 V more bias when Au atoms are pulled from AuNP (V > 0, ①) rather than from a substrate (V < 0, ②) as visualized in Figure 5b. Since ligands impede the movement of Au atoms, they can introduce a "semimemristive" effect while stopping Au from retracting back to AuNP (black arrows in Figure 5). In

**ADVANCED
SCIENCE NEWS**

www.advancedsciencenews.com

**ADVANCED
MATERIALS**

www.advmat.de

Figure 5. Understanding of electrical switching in MoS_2 nanosheets. a) Representative J–V characteristics reveal a volatile threshold process, the insert presents data plotted with log J. b) Resistivity change is driven by atomic-size Au filaments penetrating spaces between atoms in MoS_2. ① Citrate ligands impede Au migration (higher switching voltages) and prevent Au retraction introducing a stochastic "semi-nonvolatility" (black arrows). ② Au atoms pulled from Au substrate result in a reproducible sharp threshold switching.

fact, most groups observe only volatile electrical switching in nanosheet MoS_2,[23–25] and it is possible that the observation of nonvolatility in few layers thick MoS_2[13] might be associated with adlayers or transfer residues similar to citrate ligands. Indeed, it has been explicitly reported that memristive switching in vertically biased MoS_2 occurs only for a stack of monolayers,[17] thus when nanosheets are separated by transfer residues. This underlines that adlayer engineering might be a route to introduce a memristive effect in MoS_2. Nevertheless, pristine MoS_2 provides superb sharp reproducible volatile switching characteristics with negligible leakage currents. It can be thus facilitated as a very successful electrical switch or a selector to solve sneak path problems occurring in memristive crossbar arrays.[68]

We would like to highlight that although participation of V_S in metal intercalation has been proposed by many groups,[5,13,17,18,20] we are the first to explicitly image the phenomenon in ambient conditions[18,20] and suggest that metal intercalation seems to be independent from V_S. We take into consideration that small modifications in Raman[42,49] and PL[39,40] associated with V_S might be present but undetectable. However, we believe that the used combination of three independent methods lowers chances of missing the signal change. Furthermore, defect-induced alterations in Raman has been previously reported using method with sensitivity alike ours.[50] Finally, FDTD simulations estimate up to 150 intercalating nanofilaments (Figure 4d), which corresponds to ≈2% of device's area, and the passivation of 2% concentration of V_S is detectable in PL.[40]

Our discussion may apply to all transition metal dichalcogenides (TMD) due to comparable physical properties (energy structure, interatomic distances, chemical affinities etc.),[69,70] but it should not be generalized to all 2D materials, such as h-BN or graphene, which are not semiconductors. Indeed, literature data on memristive behavior for all TMD nanosheets is alike for MoS_2.[13,67,71,72] In general, nonvolatility in a few layers thick TMD was observed by only one group and a memristive switching is usually mediated by some adlayers.[13,67,71,72] The techniques involve stacking many nanosheets using wet deposition (Ag/WSe_2/Ag[67] and Pd/WS_2/Pt[73] cells), placing SiO_2 or Al_2O_3 layer on top of $MoTe_2$ (Ti/$MoTe_2$/Al_2O_3/Au and Ti/$MoTe_2$/SiO_2/Au switches),[74] and surface oxidation of WSe_2 (Ag/WO_{3-x}/WSe_2/graphene device).[71]

Finally, we note that the electrode's material may affect the switching.[12,17] Here, we test Au to reproduce the architecture of the MoS_2 atomristors[20] and to achieve plasmonic enhancement. Although Au is less prone to intercalate into MoS_2 than other active metals,[17,18] e.g., Ag[5,18,23,24] and Cu,[17] we still observe metallic ion migration, with voltages higher than those reported for those electrode materials. This implies that the switching mechanism proposed here applies to other metallic contacts. Migration of metallic ions into MoS_2 has been observed not only for Ag[5,18] and Cu[17] but also for metals (e.g., Pt[75]) less prone to intercalate than Au. In general, it seems that metal intercalation is the only mechanism triggering memristive switching of vertically biased pristine MoS_2 nanosheets as the switching was not observed for nonmetallic electrodes such as carbon nanotube electrodes[18] and graphene,[12] where memristive effects may be achieved only by oxidation of MoS_2.[12]

4. Conclusion

To our knowledge, we present the first characterization of nanoscale MoS_2-based electrical switches at room temperature and in air. We propose a tool to access both PL and Raman, together with DF spectroscopy, for a true in operando investigation of MoS_2 switching mechanisms in real time. We prove that the drop in MoS_2's resistivity is triggered by Au atoms intercalating directly between Mo and S atoms forming many nanofilaments, most likely without the involvement of sulfur vacancies. We observe volatile switching with the potential for non-volatility by a careful adlayer engineering. Although a pristine MoS_2 nanosheet does not constitute a memristor, its reproducible sharp threshold switching characteristics make it a great candidate for a nanosized electrical switch or a selector eliminating leakage currents in memristive crossbars.

5. Experimental Section

Device Fabrication: At *TU Wien* single- and few-layer MoS_2 films were grown as described in,[76] see Section SD in the Supporting Information for details. Gold substrates (80 nm Au/10 nm Cr on 300 nm SiO_2/Si)

were evaporated thermally in a custom-made evaporator. The MoS_2 film was transferred from the sapphire substrate onto the Au surface in a vacuum chamber, following the procedure.[61] For this purpose, a solution of polystyrene in toluene was spin-coated onto MoS_2 film. To delaminate the polymer film, the sample was immersed in a 30% solution of KOH. After delamination, the carrier polystyrene film was rinsed with MoS_2 film several times in DI water. To improve the adhesion between the carrier polymer film and the substrate, the sample was baked at 150 °C for ≈1 h. The polystyrene carrier film was then dissolved in toluene. Next, AuNPs (80 nm in diameter, *BBI Solutions*) were drop-casted onto the MoS_2 transferred on Au. Finally, an insulating PMMA layer was spin-coated and was etched down to ≈40 nm as confirmed on Si control samples by ellipsometry (J.A. Woollam, EC-400, 75 W Xe light source).

Electrical Setup: Biasing was achieved by contacting a single AuNP with a tipless semi-transparent cantilever (*Apex Probes*) coated by 3 nm Cr/6 nm Au (thermal evaporation). The cantilever was attached via a silver paste (SCP26G from *Electrolube*) to a custom mount operated by XYZR piezoelectric positioners (from *SmartAct*). The pressure of the top contact onto AuNP was ≈0.037 GPa, which did not affect the switching mechanism as reported.[29] The density of 1 AuNP / 100 μm^2 allowed for an electrical contact of a single AuNP (cantilever's dimensions are 30 μm × 100 μm). Electrical contact with the bottom Au substrate was achieved via a tungsten probe tip from *Lambda Photometrics Ltd* connected to a custom-made XYZ manual positioner from *Thorlabs*. Electrical signals from electrodes were sent via triaxial cables to the *Keithley 2634B* source meter, which allowed for low noise measurement down to 10 pA.

Optical Setup: The experiments were performed on the custom-made optical rig. All spectra were collected with a 2 s integration time utilizing a 100 × 0.8-NA objective from *Olympus* (LPMlanFLN). 633 and 444 nm CW single-longitudinal-mode lasers (*Integrated Optics*) were used for PL measurements. The laser power on samples was 1.5 μW. The 633-nm-excitation signals (PL/Raman) were sent into a spectrometer (*Andor*) coupled to a *Newton EMCCD* camera from *Oxford Instruments*. The 444 nm PL and DF signals were collected by an optical fiber to a dedicated spectrometer.

FDTD Simulations: Commercial *Lumerical* software from *Ansys* was used.[63] For all FDTD simulations AuNP's diameter was set to 80 nm with fixed facet diameter of 30 nm. To imitate used microscope configuration, light was injected at 55° with respect to a substrate. Complex permittivity of materials was taken from ref. [77] for Au and ref. [78] for MoS_2 (3 layers). Additionally, it was verified that MoS_2 refractive reported in other publications[79,80] gave same results. Based on literature values for PMMA,[81] polystyrene,[82,83] and citrate[84] the refractive index was set of ligand and transfer residues layers to $n = 1.5$. Based on the experimental data, for simulations of intercalating Au atoms a layout was used with 2 nm of MoS_2, 0.5 nm of ligands surrounding AuNP, and 1 nm for transfer residues under MoS_2. Intercalating filaments were simulated as cuboids (to avoid meshing errors) evenly distributed under AuNP's facet.

Supporting Information

Supporting Information is available from the Wiley Online Library or from the author.

Acknowledgements

Conflict of Interest

The authors declare no conflict of interest.

Data Availability Statement

The data that support the findings of this study are openly available in Apollo at https://doi.org/10.17863/CAM.89994, reference number 6317837.

Keywords

[1] S. Yin, C. Song, Y. Sun, L. Qiao, B. Wang, Y. Sun, K. Liu, F. Pan, X. Zhang, *ACS Appl. Mater. Interfaces* **2019**, *11*, 43344.

[2] S. M. Shinde, G. Kalita, M. Tanemura, *J. Appl. Phys.* **2014**, *116*, 214306.

[3] V. K. Sangwan, D. Jariwala, I. S. Kim, K.-S. Chen, T. J. Marks, L. J. Lauhon, M. C. Hersam, *Nat. Nanotechnol.* **2015**, *10*, 403.

[4] X. Zhu, X. Li, X. Liang, W. D. Lu, *Nat. Mater.* **2019**, *18*, 141.

[5] K. Ranganathan, M. Fiegenbaum-Raz, A. Ismach, *Adv. Funct. Mater.* **2020**, *30*, 2005718.

[6] A. A. Bessonov, M. N. Kirikova, D. I. Petukhov, M. Allen, T. Ryhänen, M. J. A. Bailey, *Nat. Mater.* **2015**, *14*, 199.

[7] P. Cheng, K. Sun, Y. H. Hu, *Nano Lett.* **2016**, *16*, 572.

[8] A. J. Arnold, A. Razavieh, J. R. Nasr, D. S. Schulman, C. M. Eichfeld, S. Das, *ACS Nano* **2017**, *11*, 3110.

[9] S. Hao, X. Ji, F. Liu, S. Zhong, K. Y. Pang, K. G. Lim, T. C. Chong, R. Zhao, *ACS Appl. Nano Mater.* **2021**, *4*, 1766.

[10] D. Li, B. Wu, X. Zhu, J. Wang, B. Ryu, W. D. Lu, W. Lu, X. Liang, *ACS Nano* **2018**, *12*, 9240.

[11] M. Chen, H. Nam, S. Wi, G. Priessnitz, I. M. Gunawan, X. Liang, *ACS Nano* **2014**, *8*, 4023.

[12] M. Wang, S. Cai, C. Pan, C. Wang, X. Lian, Y. Zhuo, K. Xu, T. Cao, X. Pan, B. Wang, S.-J. Liang, J. J. Yang, P. Wang, F. Miao, *Nat. Electron.* **2018**, *1*, 130.

[13] R. Ge, X. Wu, L. Liang, S. M. Hus, Y. Gu, E. Okogbue, H. Chou, J. Shi, Y. Zhang, S. K. Banerjee, Y. Jung, J. C. Lee, D. Akinwande, *Adv. Mater.* **2021**, *33*, 2007792.

[14] R. Ge, X. Wu, M. Kim, J. Shi, S. Sonde, L. Tao, Y. Zhang, J. C. Lee, D. Akinwande, *Nano Lett.* **2018**, *18*, 434.

[15] M. Kim, R. Ge, X. Wu, X. Lan, J. Tice, J. C. Lee, D. Akinwande, *Nat. Commun.* **2018**, *9*, 2524.

[16] M. Lanza, F. Hui, C. Wen, A. C. Ferrari, *Adv. Mater.* **2022**, https://doi.org/10.1002/adma.202205402.

[17] R. Xu, H. Jang, M.-H. Lee, D. Amanov, Y. Cho, H. Kim, S. Park, H. Shin, D. Ham, *Nano Lett.* **2019**, *19*, 2411.

[18] X. Feng, Y. Li, L. Wang, S. Chen, Z. G. Yu, W. C. Tan, N. Macadam, G. Hu, L. Huang, L. Chen, X. Gong, D. Chi, T. Hasan, A. V.-Y. Thean, Y.-W. Zhang, K.-W. Ang, *Adv. Electron. Mater.* **2019**, *5*, 1900740.

[19] X. Huang, B. Zheng, Z. Liu, C. Tan, J. Liu, B. Chen, H. Li, J. Chen, X. Zhang, Z. Fan, W. Zhang, Z. Guo, F. Huo, Y. Yang, L.-H. Xie, W. Huang, H. Zhang, *ACS Nano* **2014**, *8*, 8695.

[20] S. M. Hus, R. Ge, P.-A. Chen, L. Liang, G. E. Donnelly, W. Ko, F. Huang, M.-H. Chiang, A.-P. Li, D. Akinwande, *Nat. Nanotechnol.* **2021**, *16*, 58.

[21] D. A. B. Miller, *Proc. IEEE* **2009**, *97*, 1166.

[22] I. K. Schuller, R. Stevens, R. Pino, M. Pechan, *Neuromorphic Computing – From Materials Research to Systems Architecture Roundtable*, USDOE Office Of Science (SC), USA **2015**.

[23] M. Farronato, M. Melegari, S. Ricci, S. Hashemkhani, A. Bricalli, D. Ielmini, *Adv. Electron. Mater.* **2022**, *8*, 2101161.

[24] D. Dev, A. Krishnaprasad, M. S. Shawkat, Z. He, S. Das, D. Fan, H.-S. Chung, Y. Jung, T. Roy, *IEEE Electron Device Lett.* **2020**, *41*, 936.

[25] Q. Hua, G. Gao, C. Jiang, J. Yu, J. Sun, T. Zhang, B. Gao, W. Cheng, R. Liang, H. Qian, W. Hu, Q. Sun, Z. L. Wang, H. Wu, *Nat. Commun.* **2020**, *11*, 6207.

[26] S. Hao, X. Ji, S. Zhong, K. Y. Pang, K. G. Lim, T. C. Chong, R. Zhao, *Adv. Electron. Mater.* **2020**, *6*, 1901335.

[27] M. Lanza, H.-S. P. Wong, E. Pop, D. Ielmini, D. Strukov, B. C. Regan, L. Larcher, M. A. Villena, J. J. Yang, L. Goux, A. Belmonte, Y. Yang, F. M. Puglisi, J. Kang, B. Magyari-Köpe, E. Yalon, A. Kenyon, M. Buckwell, A. Mehonic, A. Shluger, H. Li, T.-H. Hou, B. Hudec, D. Akinwande, R. Ge, S. Ambrogio, J. B. Roldan, E. Miranda, J. Suñé, K. L. Pey, et al, *Adv. Electron. Mater.* **2019**, *5*, 1800143.

[28] G. Di Martino, S. Tappertzhofen, S. Hofmann, J. Baumberg, *Small* **2016**, *12*, 1334.

[29] G. Di Martino, A. Demetriadou, W. Li, D. Kos, B. Zhu, X. Wang, B. de Nijs, H. Wang, J. MacManus-Driscoll, J. J. Baumberg, *Nat. Electron.* **2020**, *3*, 687.

[30] D. Kos, G. Di Martino, A. Boehmke, B. de Nijs, D. Berta, T. Földes, S. Sangtarash, E. Rosta, H. Sadeghi, J. J. Baumberg, *Nat. Commun.* **2020**, *11*, 5905.

[31] P. K. Aravind, A. Nitzan, H. Metiu, *Surf. Sci.* **1981**, *110*, 189.

[32] P. K. Aravind, R. W. Rendell, H. Metiu, *Chem. Phys. Lett.* **1982**, *85*, 396.

[33] F. Benz, R. Chikkaraddy, A. Salmon, H. Ohadi, B. de Nijs, J. Mertens, C. Carnegie, R. W. Bowman, J. J. Baumberg, *J. Phys. Chem. Lett.* **2016**, *7*, 2264.

[34] I. Irfan, S. Golovynskyi, M. Bosi, L. Seravalli, O. A. Yeshchenko, B. Xue, D. Dong, Y. Lin, R. Qiu, B. Li, J. Qu, *J. Phys. Chem. C* **2021**, *125*, 4119.

[35] H. Li, Q. Zhang, C. C. R. Yap, B. K. Tay, T. H. T. Edwin, A. Olivier, D. Baillargeat, *Adv. Funct. Mater.* **2012**, *22*, 1385.

[36] J. Hong, Z. Hu, M. Probert, K. Li, D. Lv, X. Yang, L. Gu, N. Mao, Q. Feng, L. Xie, J. Zhang, D. Wu, Z. Zhang, C. Jin, W. Ji, X. Zhang, J. Yuan, Z. Zhang, *Nat. Commun.* **2015**, *6*, 6293.

[37] H. Qiu, T. Xu, Z. Wang, W. Ren, H. Nan, Z. Ni, Q. Chen, S. Yuan, F. Miao, F. Song, G. Long, Y. Shi, L. Sun, J. Wang, X. Wang, *Nat. Commun.* **2013**, *4*, 2642.

[38] W. Zhou, X. Zou, S. Najmaei, Z. Liu, Y. Shi, J. Kong, J. Lou, P. M. Ajayan, B. I. Yakobson, J.-C. Idrobo, *Nano Lett.* **2013**, *13*, 2615.

[39] T. Verhagen, V. L. P. Guerra, G. Haider, M. Kalbac, J. Vejpravova, *Nanoscale* **2020**, *12*, 3019.

[40] H. Bretscher, Z. Li, J. Xiao, D. Y. Qiu, S. Refaely-Abramson, J. A. Alexander-Webber, A. Tanoh, Y. Fan, G. Delport, C. A. Williams, S. D. Stranks, S. Hofmann, J. B. Neaton, S. G. Louie, A. Rao, *ACS Nano* **2021**, *15*, 8780.

[41] K. M. McCreary, A. T. Hanbicki, S. V. Sivaram, B. T. Jonker, *APL Mater.* **2018**, *6*, 111106.

[42] W. M. Parkin, A. Balan, L. Liang, P. M. Das, M. Lamparski, C. H. Naylor, J. A. Rodríguez-Manzo, A. T. C. Johnson, V. Meunier, M. Drndić, *ACS Nano* **2016**, *10*, 4134.

[43] H. Nan, Z. Wang, W. Wang, Z. Liang, Y. Lu, Q. Chen, D. He, P. Tan, F. Miao, X. Wang, J. Wang, Z. Ni, *ACS Nano* **2014**, *8*, 5738.

[44] X. Wei, Z. Yu, F. Hu, Y. Cheng, L. Yu, X. Wang, M. Xiao, J. Wang, X. Wang, Y. Shi, *AIP Adv.* **2014**, *4*, 123004.

[45] B. Chakraborty, A. Bera, D. V. S. Muthu, S. Bhowmick, U. V. Waghmare, A. K. Sood, *Phys. Rev. B* **2012**, *85*, 161403.

[46] Y. Yu, G.-H. Nam, Q. He, X.-J. Wu, K. Zhang, Z. Yang, J. Chen, Q. Ma, M. Zhao, Z. Liu, F.-R. Ran, X. Wang, H. Li, X. Huang, B. Li, Q. Xiong, Q. Zhang, Z. Liu, L. Gu, Y. Du, W. Huang, H. Zhang, *Nat. Chem.* **2018**, *10*, 638.

[47] U. Bhanu, M. R. Islam, L. Tetard, S. I. Khondaker, *Sci. Rep.* **2015**, *4*, 5575.

[48] K. Gołasa, M. Grzeszczyk, J. Binder, R. Bożek, A. Wysmołek, A. Babiński, *AIP Adv.* **2015**, *5*, 077120.

[49] G. L. Frey, R. Tenne, M. J. Matthews, M. S. Dresselhaus, G. Dresselhaus, *Phys. Rev. B* **1999**, *60*, 2883.

[50] T.-X. Huang, X. Cong, S.-S. Wu, K.-Q. Lin, X. Yao, Y.-H. He, J.-B. Wu, Y.-F. Bao, S.-C. Huang, X. Wang, P.-H. Tan, B. Ren, *Nat. Commun.* **2019**, *10*, 5544.

[51] C. Tan, H. Zhang, *Chem. Soc. Rev.* **2015**, *44*, 2713.

[52] K. F. Mak, K. He, C. Lee, G. H. Lee, J. Hone, T. F. Heinz, J. Shan, *Nat. Mater.* **2013**, *12*, 207.

[53] N. Scheuschner, O. Ochedowski, A.-M. Kaulitz, R. Gillen, M. Schleberger, J. Maultzsch, *Phys. Rev. B* **2014**, *89*, 125406.

[54] C. Lumdee, B. Yun, P. G. Kik, *ACS Photonics* **2014**, *1*, 1224.

[55] M. R. Beversluis, A. Bouhelier, L. Novotny, *Phys. Rev. B* **2003**, *68*, 115433.

[56] B. Chakraborty, H. S. S. R. Matte, A. K. Sood, C. N. R. Rao, *J. Raman Spectrosc.* **2013**, *44*, 92.

[57] M. Buscema, G. A. Steele, H. S. J. van der Zant, A. Castellanos-Gomez, *Nano Res.* **2014**, *7*, 561.

[58] G. Milano, M. Luebben, M. Laurenti, L. Boarino, C. Ricciardi, I. Valov, *Adv. Mater. Interfaces* **2021**, *8*, 2100915.

[59] D.-B. Grys, B. de Nijs, A. R. Salmon, J. Huang, W. Wang, W.-H. Chen, O. A. Scherman, J. J. Baumberg, *ACS Nano* **2020**, *14*, 8689.

[60] J.-W. Park, J. S. Shumaker-Parry, *J. Am. Chem. Soc.* **2014**, *136*, 1907.

[61] A. Gurarslan, Y. Yu, L. Su, Y. Yu, F. Suarez, S. Yao, Y. Zhu, Y. Ozturk, Y. Zhang, L. Cao, *ACS Nano* **2014**, *8*, 11522.

[62] Y. Shen, W. Zheng, K. Zhu, Y. Xiao, C. Wen, Y. Liu, X. Jing, M. Lanza, *Adv. Mater.* **2021**, *33*, 2103656.

[63] Ansys Lumerical FDTD | Simulation for Photonic Components, https://www.ansys.com/products/photonics/fdtd (accessed: September 2022).

[64] J. C. Slater, *J. Chem. Phys.* **1964**, *41*, 3199.

[65] J. Xiao, M. Long, X. Li, Q. Zhang, H. Xu, K. S. Chan, *J. Phys.: Condens. Matter* **2014**, *26*, 405302.

[66] J. S. Lee, S. Lee, T. W. Noh, *Appl. Phys. Rev.* **2015**, *2*, 031303.

[67] M. Sivan, Y. Li, H. Veluri, Y. Zhao, B. Tang, X. Wang, E. Zamburg, J. F. Leong, J. X. Niu, U. Chand, A. V.-Y. Thean, *Nat. Commun.* **2019**, *10*, 5201.

[68] S. H. Chang, S. B. Lee, D. Y. Jeon, S. J. Park, G. T. Kim, S. M. Yang, S. C. Chae, H. K. Yoo, B. S. Kang, M.-J. Lee, T. W. Noh, *Adv. Mater.* **2011**, *23*, 4063.

[69] S. Manzeli, D. Ovchinnikov, D. Pasquier, O. V. Yazyev, A. Kis, *Nat. Rev. Mater.* **2017**, *2*, 17033.

[70] J. Zhou, J. Lin, X. Huang, Y. Zhou, Y. Chen, J. Xia, H. Wang, Y. Xie, H. Yu, J. Lei, D. Wu, F. Liu, Q. Fu, Q. Zeng, C.-H. Hsu, C. Yang, L. Lu, T. Yu, Z. Shen, H. Lin, B. I. Yakobson, Q. Liu, K. Suenaga, G. Liu, Z. Liu, *Nature* **2018**, *556*, 355.

[71] W. Huh, S. Jang, J. Y. Lee, D. Lee, D. Lee, J. M. Lee, H.-G. Park, J. C. Kim, H. Y. Jeong, G. Wang, C.-H. Lee, *Adv. Mater.* **2018**, *30*, 1801447.

[72] W. Huh, D. Lee, C.-H. Lee, *Adv. Mater.* **2020**, *32*, 2002092.

[73] X. Yan, Q. Zhao, A. P. Chen, J. Zhao, Z. Zhou, J. Wang, H. Wang, L. Zhang, X. Li, Z. Xiao, K. Wang, C. Qin, G. Wang, Y. Pei, H. Li, D. Ren, J. Chen, Q. Liu, *Small* **2019**, *15*, 1901423.

**ADVANCED
SCIENCE NEWS**

www.advancedsciencenews.com

**ADVANCED
MATERIALS**

www.advmat.de

[74] F. Zhang, H. Zhang, S. Krylyuk, C. A. Milligan, Y. Zhu, D. Y. Zemlyanov, L. A. Bendersky, B. P. Burton, A. V. Davydov, J. Appenzeller, *Nat. Mater.* **2019**, *18*, 55.

[75] S. Yin, Z. Luo, Q. Li, C. Xiong, Y. Liu, R. Singh, F. Zeng, Y. Zhong, X. Zhang, *Phys. Status Solidi A* **2019**, *216*, 1900104.

[76] D. Dumcenco, D. Ovchinnikov, K. Marinov, P. Lazić, M. Gibertini, N. Marzari, O. L. Sanchez, Y.-C. Kung, D. Krasnozhon, M.-W. Chen, S. Bertolazzi, P. Gillet, A. Fontcuberta i Morral, A. Radenovic, A. Kis, *ACS Nano* **2015**, *9*, 4611.

[77] P. B. Johnson, R. W. Christy, *Phys. Rev. B* **1972**, *6*, 4370.

[78] B. Song, H. Gu, M. Fang, X. Chen, H. Jiang, R. Wang, T. Zhai, Y.-T. Ho, S. Liu, *Adv. Opt. Mater.* **2019**, *7*, 1801250.

[79] K. M. Islam, R. Synowicki, T. Ismael, I. Oguntoye, N. Grinalds, M. D. Escarra, *Adv Photonics Res* **2021**, *2*, 2000180.

[80] C. Hsu, R. Frisenda, R. Schmidt, A. Arora, S. M. de Vasconcellos, R. Bratschitsch, H. S. J. van der Zant, A. Castellanos-Gomez, *Adv. Opt. Mater.* **2019**, *7*, 1900239.

[81] Kayaku Advanced Materials, "PMMA Positive Resists", https://kayakuam.com/products/pmma-positive-resists/ (accessed: September 2022).

[82] N. Sultanova, S. Kasarova, I. Nikolov, *Acta Phys. Pol. A* **2009**, *116*, 585.

[83] X. Zhang, J. Qiu, X. Li, J. Zhao, L. Liu, *Appl. Opt.* **2020**, *59*, 2337.

[84] PubChem, "Citric Acid", https://pubchem.ncbi.nlm.nih.gov/compound/311 (accessed: October 2022).

2209968 (9 of 9)